Polymer Testing 93 (2021) 106961

Contents lists available at ScienceDirect

Polymer Testing

journal homepage: http://www.elsevier.com/locate/polytest

# Thermo-resistive and thermo-piezoresistive sensitivity of carbon nanostructure engineered thermoplastic composites processed via additive manufacturing

Pawan Verma [a], Andreas Schiffer [b], S. Kumar [c,*]

[a] Artie McFerrin Department of Chemical Engineering, Texas A&M University, College Station, TX, 77840, USA
[b] Department of Mechanical Engineering, Khalifa University of Science and Technology, 127788, Abu Dhabi, United Arab Emirates
[c] James Watt School of Engineering, University of Glasgow, Glasgow, G12 8LT, UK

ARTICLE INFO

*Keywords:*
Temperature sensing
Strain sensing
3D printing
Multifunctional composites
Fused filament fabrication

ABSTRACT

We experimentally examine the thermo-resistive and thermo-piezoresistive sensitivity of multiwall carbon nanotube (MWCNT)/polypropylene random copolymer (PPR) nanocomposites processed via fused filament fabrication (FFF) process. The filament feedstocks were fabricated by melt blending of neat PPR with a predetermined amount of MWCNTs (either 4, 6 or 8 wt%) using a twin-screw extruder. Thermo-resistive characteristics of MWCNT/PPR composites were measured under both constrained and unconstrained heating from approximately 30-100 °C. For all MWCNT concentrations considered here, negative temperature coefficients of resistivity (TCR) were observed for both constrained and unconstrained heating, as a consequence of thermal fluctuation-induced tunneling at MWCNT junctions. The highest thermo-resistive sensitivity was measured for the composite with the lowest MWCNT concentration (4 wt%) under unconstrained conditions, reporting a TCR of $-12{,}800 \times 10^{-6}$/°C, which is higher in magnitude than that of other polymer nanocomposites reported in the literature. Moreover, the MWCNT/PPR composites exhibit strong thermo-piezoresistive response under tensile loading. For 4 wt% MWCNT loading, the gauge factor (measured over 0–20% strain range) of the composite increased from 27.8 to 52.3 when the temperature was raised from 30 °C to 60 °C. Our results further evince higher thermo-piezoresistive sensitivity i.e., a gauge factor as high as 395 at 60 °C. The electron tunneling and hopping, both thermally-assisted and activated by mechanical deformation of the PPR matrix, significantly increase the thermo-piezoresistance with the increase in temperature in this range. The excellent thermo-resistive and thermo-piezoresistive characteristics of MWCNT/PPR composites reported in this study would enable the development of smart nanocomposites for self-sensing both temperature and strain/damage state.

## 1. Introduction

The development of polymer-based nanocomposites with multifunctional attributes has been a research topic of great technological and scientific interest over the last decade. These materials typically consist of a network of highly conductive nanofillers (e.g. carbon nanotubes, carbon black, graphene, etc.) embedded in an electrically non-conducting polymer matrix. The mechanical and physical properties of such electro-conductive composites are sensitive to external stimuli, making them candidate materials for temperature-, pressure- and strain-sensing applications [1–8]. Carbon nanotubes (CNTs) have been most prominent in the development of highly-conducting polymer-based composites for sensing applications. CNTs have a long tube-like structure, ultra-high elastic modulus (~1.0 TPa), strength (~100 GPa) and outstanding thermal (3000–6000 W/mK) and electrical conductivity ($10^4$–$10^6$ S/cm) [9,10]. The high aspect ratio of CNTs is attributed to the formation of conducting 3D networks and concomitant low-percolation thresholds [9,11,12]. The conducting composite can be fabricated by mixing an adequate amount of CNTs with the polymer via different blending techniques to obtain a uniform dispersion of nanofillers in the polymer matrix and to achieve electrical percolation [10,13].

Additive manufacturing (AM) [14–18], also known as 3D printing, is an emerging technique for processing of materials, including polymer-based composites. The major advantage of AM is that it enables fabrication of objects with complex shapes or topology, offering

* Corresponding author.
*E-mail address:* s.kumar@eng.oxon.org (S. Kumar).

https://doi.org/10.1016/j.polymertesting.2020.106961
Received 2 May 2020; Received in revised form 6 November 2020; Accepted 10 November 2020
Available online 18 November 2020

flexibility to modify the geometry without the need for additional tooling. Different types of AM techniques such as stereolithography (SLA) [19–24], fused filament fabrication (FFF) [25–33], selective laser sintering (SLS) [33,34], inkjet printing, selective laser melting (SLM) [35–38] etc., enable 3D printing of different classes of materials. The FFF AM is extensively being used for processing polymer composites due to its simplicity, high reliability and comparatively low operational and machine costs [12,39–43]. The feedstock used in the FFF process is a continuous filament of a uniform diameter, which was prepared via melt extrusion process. Mostly acrylonitrile butadiene (ABS) [44,45], polylactic acid (PLA) [46], polyamide (PA) [47], polycarbonate (PC) [48], and polystyrene (PS) [49] and their composites are processed via FFF 3D printing.

Composites composed of polymers with dispersed CNTs typically possess strongly pronounced piezoresistive behavior above the percolation threshold [50], making them suitable for strain sensing applications that require a high degree of compliance or stretchability (e.g. human-machine interfaces). Their piezoresistive behavior is primarily ascribed to deformation-induced widening/closing of the tunneling gaps between CNT junctions, leading to an increase/decrease in the resistivity of the material [51]. The effect of temperature on the electrical resistivity of a polymer-based nanocomposite, also known as thermo-resistivity, has been studied by several authors [52–61]. The sensitivity of a material's electrical resistivity to variations in temperature is an important consideration for the development of temperature sensors (or thermistors), and is typically referred to as temperature coefficient of resistance (TCR) [62]. The thermo-resistive behavior of polymer nanocomposites filled with micro/nano conductive fillers has been found to depend on the filler concentration [53], temperature [63] and properties of the polymer matrix [64]. Both positive [58–60] and negative TCR [55–57,61] have been reported for CNT/polymer composites. For example, Lasater and Thostenson [52] examined the thermos-resistive behavior of CNT/vinyl ester composites and found both positive and negative TCR depending on the CNT concentration and temperature. Other authors [54] measured thermo-resistive properties of MWCNT/PSF composites with MWCNT concentrations ranging between 0.5 and 50 wt%. For composites with large MWCNT loadings (40 wt% and above), they observed negative TCR while those with lower MWCNT concentrations exhibited positive TCR, concluding that the thermo-resistance of CNT/polymer composites undergoes a transition from thermal expansion-controlled behavior at low MWCNT loading (positive TCR) to the one dominated by the intrinsic thermo-resistivity of MWCNTs [65,66] at high MWCNT loading (negative TCR). Similar findings were also obtained numerically [53]. Predominantly negative TCR values were reported, for example, by Shen et al. [61] for nano-carbon/epoxy composites, Mohiuddin and Hoa [56] for CNT/PEEK and Matzeu et al. [57] for MWCNT/SEBS. The observed trends were ascribed to changes in thermal fluctuation-induced tunneling conduction with increasing temperature [61], outweighing the increase in tunneling resistance of the CNT network due to thermal expansion. It was also noted in Ref. [61] that a high degree of CNT entanglement in the polymer matrix may also contribute to a negative TCR, since it allows tunneling gaps to be reduced despite the fact that the polymer matrix is expanding with increasing temperature.

Although the studies outlined above have examined the thermo-resistive responses of different types of CNT/polymer composites and studied the underlying mechanisms, the degree to which these novel material systems can be used in conjunction with 3D printing has not yet been demonstrated. Furthermore, only a very limited data is currently available on the thermo-piezoresistive response of CNT/polymer composites which is an important aspect in the design of strain sensors or self-sensing structural systems exposed to a wider range of temperatures. Here, we study experimentally the thermo-resistive response of 3D printed multi-walled carbon nanotube (MWCNT)/polypropylene random copolymer (PPR) composites and explore the effect of temperature on their piezoresistive performance. The composite specimens are processed via FFF AM with the feedstock filaments prepared through melt blending of neat PPR with a predetermined amount of MWCNT nanofillers (either 4, 6 or 8 wt%) using a twin-screw extruder. The change in the electrical resistance of 3D printed MWCNT/PPR composites with temperature is measured under constrained and unconstrained conditions and their TCR is evaluated and compared to previously published work. In addition, the piezoresistive and mechanical responses of the MWCNT/PPR composites are measured at 30, 60 and 100 °C and the corresponding gauge factors are deduced from the measurements. The results obtained from this study serve as guidelines for the development of advanced 3D printed CNT/polymer composites for temperature- and strain-sensing applications.

## 2. Materials and experimental methods

### 2.1. Materials

MWCNTs supplied by Applied Nanostructured Solution LLC were used as conducting fillers. The length and average outer diameter of these MWCNTs were reported in Ref. [67] as ≈ 30 μm and 10–12 nm, respectively. PPR having a melt flow index of 0.3 g/10 min (at 230°C/2.16 kg) was procured from Borouge Pte Ltd. According to DSC scans, the melting and crystalline temperatures of the PPR are 147 °C and 112 °C, respectively, and the degree of crystallinity is 30.8%. The DSC thermographs and a description of the experimental procedure are presented in Section S1 (Supplementary Information).

### 2.2. Preparation of MWCNT/PPR composite filaments for 3D printing

The 3D printable MWCNT/PPR composite filaments were fabricated by melt blending the neat PPR with a predetermined amount of MWCNT nanofillers (either 4, 6 or 8 wt%) in a corotating twin-screw extruder (Coperion ZSK 18 Germany) having $L/D = 40$ ($L$ is the screw length and $D$ is the screw diameter) at 200 rpm with a feed rate of 2.5 kg/h, as shown in Fig. 1. The CNT loading was limited to 8 wt% in this work, since filaments with higher CNT concentrations could not be effectively processed by this technique due to poor flow properties of the blend. The barrel temperature of the extruder was set to 180 °C in the feed zone and was gradually increased in the feed direction to reach 220 °C at the die. Note that the process parameters were kept constant for all the filaments fabricated in this study. The obtained composite filaments had a final diameter of 1.74 mm and are labelled as PPR-4, PPR-6 or PPR-8 where the numeric term indicates the MWCNT concentration in wt.%. Note that the above melt blending process resulted in a nearly uniform dispersion of MWCNTs within the filament, as seen from Fig. S2 (Supplementary Information).

### 2.3. 3D printing via fused filament fabrication (FFF)

3D printing of MWCNT/PPR nanocomposites utilizing in-house nano-engineered filaments was carried out using a Creator Pro Flash Forge 3D printer. CAD models were prepared using SolidWorks software and converted into 3D printable STL files for the preparation of test specimens. Simplify3D slicing software tool was used to convert the STL files into G-code. The MWCNT/PPR filament of 1.74 mm diameter was fed into the printer nozzle of diameter 0.4 mm by a driver motor through a counter-rotating set of grooved gears. A unidirectional infill pattern with 100% infill density was chosen with the beads aligned parallel to the loading direction of the specimen. The printing parameters were kept the same for all the samples investigated in this study and are listed in Table 1.

### 2.4. Characterization of the thermo-resistive and thermo-piezoresistive response

Three types of tests were carried out to characterize the thermo-

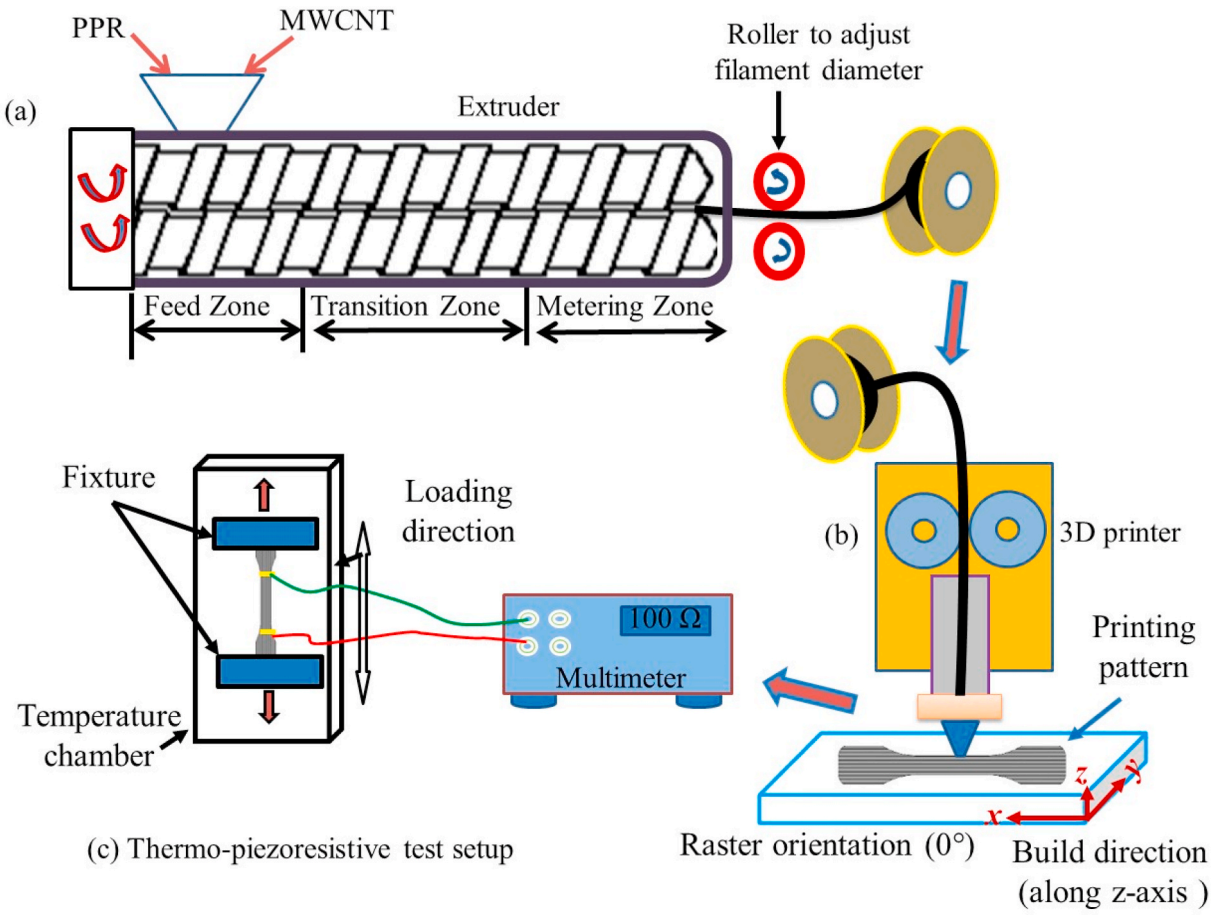


**Fig. 1.** Schematic illustration of (a) MWCNT/PPR filament fabrication, (b) 3D printing via FFF AM and (c) thermo-piezoresistive test setup.

**Table 1**
Process parameters for 3D printing of MWCNT/PPR composites via FFF.

| Process parameter | Unit | Value |
|---|---|---|
| Printing speed | mm/min | 900 |
| First layer printing speed | mm/min | 300 |
| Nozzle tip temperature | °C | 230 |
| First layer temperature | °C | 230 |
| Bed temperature | °C | 115 |
| Layer height | mm | 0.18 |
| First layer | mm | 0.18 |
| Extrusion width | mm | 0.4 |
| Filament diameter | mm | 1.74 |
| Infill density | % | 100 |

resistive and thermo-piezoresistive responses of 3D printed MWCNT/PPR composites. Three repeated tests were performed for each sample to ensure repeatability of the measurements. These are described in the following sections.

#### 2.4.1. Thermo-resistive response under unconstrained deformation

The temperature dependent electrical resistance of 3D printed MWCNT/PPR composites was measured via two-probe method using a Tektronix DMM 4050 multimeter on rectangular samples (30 mm × 5 mm × 4 mm) heated from 35 °C to 100 °C at a rate of 5 °C/min in an environmental chamber attached to an Intron universal testing machine (UTM). Prior to testing, the samples were coated with silver paste at the gauge points to ensure adequate electrical contact between the sample and the electrodes of the probe. Note that the silver paste did not have any measurable effect on the electrical resistance of the samples. The average electrical resistance $R$ of the sample was measured *in-situ* while it was allowed to freely expand during heating to guarantee stress-free conditions.

The average electrical resistance $R$ of the nanocomposite prismatic bar is given by Ref. [68,69].

$$R = \rho \frac{L}{wt} \tag{1}$$

where $\rho$ is the average electrical resistivity of the nanocomposite, and $L$, $w$ and $t$ are the sample's length, width and thickness, respectively. Noting that all the quantities on the right-hand side of eq. (1) are, in general, temperature-dependent, the temperature coefficient of resistance ($TCR$) of the nanocomposite is expressed as

$$TCR = \frac{1}{R}\frac{dR}{dT} = \frac{1}{\rho}\frac{d\rho}{dT} + \frac{1}{L}\frac{dL}{dT} - \frac{1}{w}\frac{dw}{dT} - \frac{1}{t}\frac{dt}{dT}. \tag{2}$$

Assuming that the thermal expansion of the material is isotropic, it follows that

$$\frac{1}{L}\frac{dL}{dT} = \frac{1}{w}\frac{dw}{dT} = \frac{1}{t}\frac{dt}{dT} = \alpha, \tag{3}$$

where $\alpha$ is the thermal coefficient of expansion. Using eq. (3), the TCR expression can be written in a simplified form as

$$TCR = \frac{1}{R}\frac{dR}{dT} = \frac{1}{\rho}\frac{d\rho}{dT} - \alpha. \tag{4}$$

In the limit of small changes, eq. (4) can be written as

$$TCR = \frac{\Delta R}{R_0}\frac{1}{\Delta T} = \frac{\Delta \rho}{\rho_0}\frac{1}{\Delta T} - \alpha \tag{5}$$

where $\Delta R = R - R_0$, $\Delta T = T - T_0$ and $\Delta\rho = \rho - \rho_0$. $R_0$ and $\rho_0$ are the initial electrical resistance and resistivity, respectively at $T_0$, where $T_0$ is the initial temperature. We note that the first term on the right-hand side of eq. (5) denotes the change in the composite's resistivity with temperature and includes not only the temperature dependence of the intrinsic resistivity of MWCNTs but also resistivity changes induced by widening/closing of tunneling gaps at MWCNT junctions, i. e the resistivity changes due to the change in the morphology of the MWCNT network.

#### 2.4.2. Thermo-resistive response under constrained deformation

To measure the effect of temperature on the electrical resistance of mechanically constrained MWCNT/PPR samples, we used the same test methods and materials as described in Section 2.4.1 but with the ends of the rectangular sample clamped between the wedge action grips of the Instron UTM. The force $F$ induced in the specimen during the test was measured using a 5 kN load cell and the obtained force readings were then converted into engineering stress via $\sigma = F/A_0$, where $A_0$ is the initial cross-sectional area of the specimen. Note that, under constrained conditions, $dL/dT = 0$ in eq. (2), which requires eq. (5) to be modified to

$$TCR' = \frac{\Delta R}{R_0}\frac{1}{\Delta T} = \frac{\Delta\rho}{\rho_0}\frac{1}{\Delta T} - 2\alpha \quad (6)$$

where, $TCR'$ is the temperature coefficient of resistance of the sample under constrained conditions. Moreover, the stress $\sigma$ generated in the constrained sample evolves with temperature and is equal to $E\alpha\Delta T$ before yielding. $E$ and $\alpha$ are the Young's modulus and coefficient of thermal expansion of the nanocomposite sample.

#### 2.4.3. Temperature-dependent piezoresistive response

The effect of temperature on the mechanical and piezoresistive response of MWCNT/PPR composites was measured under isothermal conditions on dogbone samples of thickness 2 mm and gauge length 30 mm according to ISO 527 (see Fig. S3, Supplementary Information) using an Instron UTM (with a 5 kN load cell) and fitted with an environmental chamber. The samples were placed between the wedge-action grips of the UTM and the crosshead was displaced at a rate of 5 mm/min to subject the specimen to uniaxial tensile loading at a strain rate of 0.0028 $s^{-1}$. To measure changes in the electrical resistance with deformation, a Tektronix DMM 4050 multimeter was used, as described in Section 2.4.1. During the test, the temperature in the chamber was kept fixed at 30, 60 or 100 °C, and the electrical resistance, crosshead displacement as well as the force induced in the specimen were recorded. The force vs. displacement curves were then converted into engineering stress vs. strain curves, assuming that all the deformation occurs within the gauge section of the specimen.

### 2.5. Thermal expansion measurements

A Dilatometer DIL 802 (TA Instruments) was used to measure the coefficient of thermal expansion of neat PPR and MWCNT/PPR composites within a temperature range of 40–80 °C, following Arief et al. [29]. Cylindrical samples of length 35 mm and diameter 5 mm were used for this purpose.

## 3. Results and discussion

### 3.1. Thermo-resistive behavior under unconstrained conditions

In Fig. 2a we plot the measured electrical resistance as a function of temperature for 3D printed MWCNT/PPR composites with 4, 6 and 8 wt % MWCNT concentration, respectively. It can be seen from Fig. 2a that all the MWCNT/PPR composites exhibit pronounced nonlinear thermo-resistive behavior with electrical resistance $R$ continuously decreasing with increasing temperature for all MWCNT concentrations considered here. Such decrease in resistance with increasing temperature is typically observed in nanocomposites with sufficiently high loading of MWCNTs, as reported in Ref. [54], where the change in electrical resistance with temperature is governed by the negative TCR of the MWCNT network, rather than by its change in morphology due to thermal expansion of the polymer matrix [54]. For the same material system, positive or negative TCR can also be observed in different temperature regimes [53]. For a given temperature change $\Delta T$, it can be seen from eq. (5), that the normalized change in electrical resistance, $\Delta R/R_0$, can be used to quantify the thermo-resistance sensitivity (or TCR) of the nanocomposite. In Fig. 2b, $\Delta R/R_0$ is plotted as a function of temperature $T$ for the three MWCNT concentrations considered here, showing that the composite with the lowest MWCNT loading (4 wt%, PPR-4) possesses the highest TCR under unconstrained conditions for $T > 55$ °C, while the PPR-8 is more sensitive at lower temperatures, $T < 55$ °C, confirming the important role of intrinsic thermo-resistivity of the MWCNT, especially at high MWCNT concentrations and low temperatures [70].

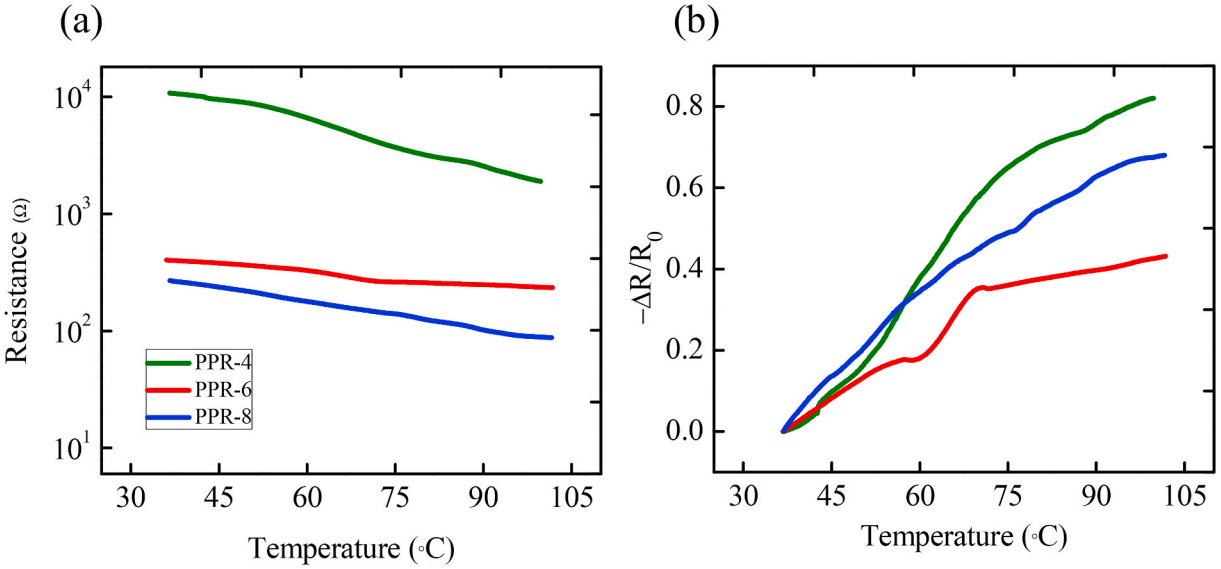


**Fig. 2.** Thermo-resistive response of MWCNT/PPR composites with 4, 6 or 8 wt% of MWCNTs: (a) Electrical resistance vs. temperature and (b) normalized change in resistance vs. temperature.

The TCR values of the MWCNT/PPR composites under unconstrained conditions were deduced from Fig. 2b by evaluating the averaged slopes of the $\Delta R/R_0$ vs. temperature curves over the measurement range (37-100 °C), and the obtained values are plotted in Fig. 3a, showing negative TCR values for all composites examined here. It is interesting to note that the composite with the lowest MWCNT loading (PPR-4) possesses the highest thermo-resistive sensitivity (TCR = $-12{,}800 \times 10^{-6}/^{o}$C), in line with the findings of previous studies [54], while the PPR-6 has the lowest sensitivity (TCR = $-6670/^{o}$C), possibly due to processing-induced differences in the dispersion of MWCNTs in the PPR matrix.

The thermal expansion coefficients $\alpha$ of the neat PPR and MWCNT/PPR composites with 4, 6 and 8 wt% MWCNT loading are plotted in Fig. 3b as a function of temperature (from 40 to 80 °C). The figure shows that the $\alpha$ values of the PPR and MWCNT/PPR composites decrease with increasing temperature and increasing MWCNT loading, due to the negative thermal expansion of MWCNTs, as reported by other authors [71,72]. Since the coefficients of thermal expansion $\alpha$ of the MWCNT/PPR composites (Fig. 3b) are substantially smaller than those reported in the literature for other CNT/polymer composites [52], the effect of thermal expansion on the tunneling and hopping resistance is expected to be small here (i. e. the resistance change due to change in morphology of MWCNT network) in comparison to the intrinsic thermo-resistivity of the MWCNTs. Therefore, we argue that the observed thermo-resistive response is controlled by the thermal fluctuation-induced tunneling conduction, as also noted by other authors [61].

### 3.2. Thermo-resistive behavior under constrained conditions

In Fig. 4a–c, we present, for the case of constrained heating, the induced stresses $\sigma$ and normalized resistance changes $\Delta R/R_0$ plotted as a function of temperature for the three MWCNT/PPR composites, PPR-4, PPR-6 and PPR-8, respectively. The plots show that, as the temperature increases, compressive (i.e. negative) stresses are induced in the samples due to constrained thermal expansion of the sample. At low temperatures, the compressive stresses generated in the sample increase with increasing temperature until a peak is reached, after which the response of the polymer becomes increasingly viscous, resulting in continuous stress relaxation with increasing temperature. The competition between the stress build-up rate and the stress relaxation rate during the constrained heating determines the peak point. The latter phenomenon can be attributed to the relaxation of the rigid amorphous phase surrounding the PP crystals, also referred to as α-relaxation, that typically occurs within a temperature range of 70–90 °C in PPR and PPR nanocomposites [73,74], while the glass transition temperature of the unconstrained amorphous phase (i.e. β-relaxation) in PPR typically occurs below room temperature at around 15–20 °C [73,74]. Similar to what is presented in Fig. 3 for the unconstrained case, the electrical resistance of the MWCNT/PPR composites decreases during constrained heating, as seen from the negative values of $\Delta R/R_0$ in Fig. 4a–c. The TCR values for constrained heating were evaluated from the $\Delta R/R_0$ vs. temperature curves in Fig. 4 (over 30-100 °C) and the obtained values were included in Fig. 3a, to compare with the corresponding TCR values evaluated under unconstrained conditions. For the PPR-4 composite, the TCR for constrained heating (see Fig. 3a) is similar to that measured under unconstrained conditions. However, the TCR values of the PPR-6 and PPR-8 under constrained conditions are significantly lower than those obtained for unconstrained heating (see Fig. 3b). This is attributed to the segmental mobility of polymer chains that drives the stress relaxation in the mechanically constrained PPR matrix above the glass transition temperature ($T_g$ = 15–20 °C), and also affects the tunneling resistance of the percolating MWCNT network [52].

### 3.3. Effect of temperature on the mechanical and piezoresistive response

We proceed to examine the effect of temperature on the stress vs. strain response and associated changes in electrical resistance of the MWCNT/PPR composites. In Fig. 5a and b, we plot, respectively, the stresses and normalized resistance changes, $\Delta R/R_0$, as functions of strain for the composite with 4 wt% MWCNT loading (PPR-4); three contours are included in each figure, representing the measurements obtained from isothermal displacement-controlled tests at 30 °C, 60 °C and 100 °C, respectively. For all the temperatures considered here, Fig. 4a shows that the mechanical response of the PPR-4 is characterized by a nearly linear initial stress-strain response followed by a yielding beyond which the flow stresses are almost insensitive to variations in the applied strain. The slight nonlinearity observed in the initial stress-strain response can be attributed to viscous relaxation processes within the amorphous phase of the PPR, while the observed yielding of the PPR-4

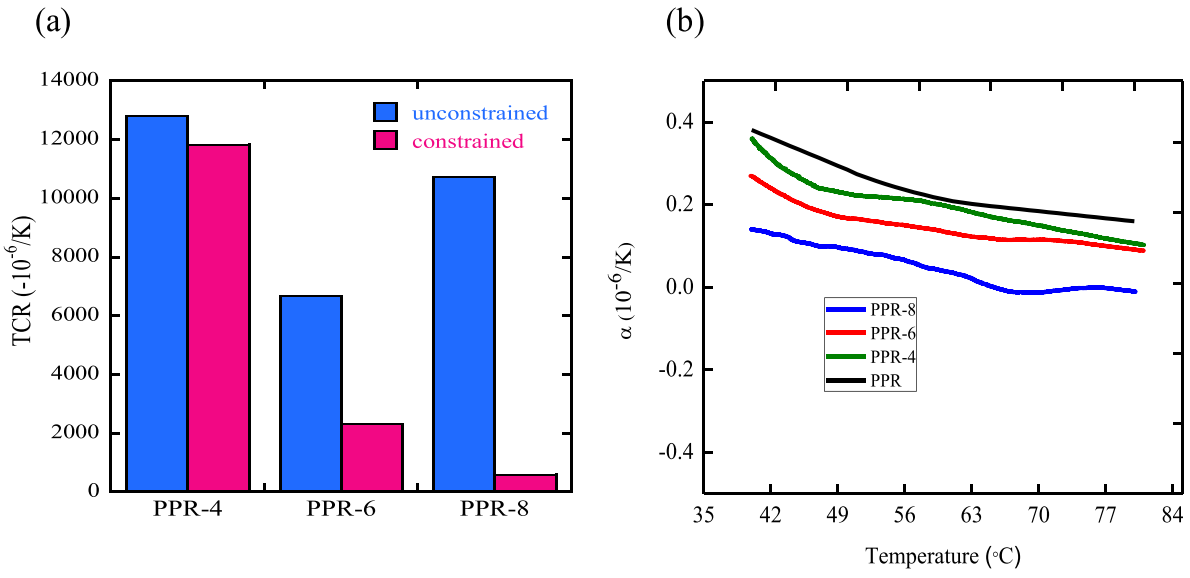


**Fig. 3.** (a) Temperature coefficient of resistance (TCR) evaluated over 37-100 °C under unconstrained and constrained conditions; (b) thermal expansion coefficient $\alpha$ of PPR and MWCNT/PPR composites with 4, 6 and 8 wt% MWCNT loading as a function of temperature.

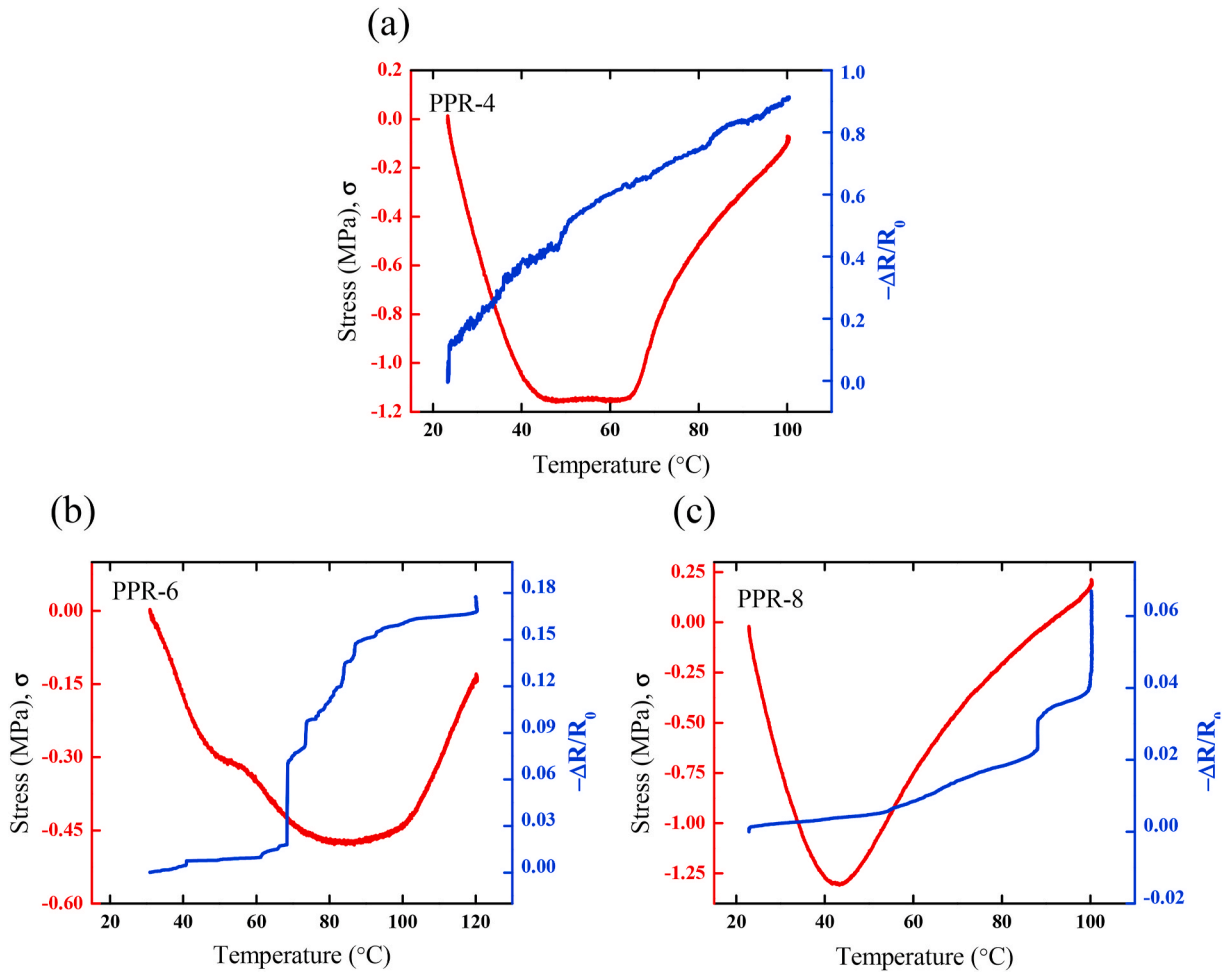


**Fig. 4.** Thermo-resistive and mechanical responses of MWCNT/PPR composites as functions of temperature under constrained deformation: (a) PPR-4, (b) PPR-6 and (c) PPR-8.

can be explained by the occurrence of stress-induced chain sliding and/or kinking processes, resulting in inelastic macroscopic deformation. It can also be seen from Fig. 5a that the induced stresses decrease significantly with increasing temperature during all stages of the response due to the concomitant increase in the chain mobility of the PPR with increasing temperature. Fig. 5b shows that the corresponding normalized resistance changes, $\Delta R/R_0$, increase monotonically with increasing strain for all choices of temperature, due to the increase of the tunneling gaps between adjacent MWCNTs with increasing tensile strain. It is interesting to note that an increase in temperature from 30 °C to 60 °C results in a more pronounced piezoresistive effect, showing higher $\Delta R/R_0$ for a wide range of strains, while a further increase of temperature to 100 °C results in a less pronounced $\Delta R/R_0$ response. This is likely due to changes in the segmental mobility of the polymer matrix which affects the tunneling resistance and perhaps, the morphology of the MWCNT network during deformation. Furthermore, the contribution of intrinsic resistivity of MWCNT to piezoresistive response of the composite at high temperature becomes less pronounced.

Similar trends are shown for the PPR-6 and PPR-8 in Fig. 5c–d and Fig. 5e–f, respectively. At $T = 30$ °C, the mechanical responses of both the PPR-6 and PPR-8 show a higher ultimate stress but decreased ductility, failing at $\varepsilon = 0.65$ and $\varepsilon = 0.33$, respectively (see Fig. 5c and e), owing to the fact that the embedded MWCNTs act as obstacles to stress-induced chain sliding in the PPR matrix, thereby increasing the resistance to inelastic deformation. These effects are less pronounced at higher temperatures, due to the increased chain mobility of the PPR matrix, offering alternative pathways for chain sliding processes.

Furthermore, the Young's moduli of the MWCNT/PPR composites were evaluated from the initial slopes of the measured stress-strain curves shown in Fig. 5 and the obtained values are summarized in Table 2, together with the ultimate strength and failure strain for each composite. Note that, at higher temperatures, some samples could not be tested until failure since the range of crosshead displacement was constrained by the limited size of the environmental chamber. Further, we note that, at 30 °C, the Young's modulus of the composite increases significantly with increasing MWCNT content, reporting a 43% difference in stiffness between the PPR-4 and the PPR-8. Such stiffening effect has been reported in previous studies [67,75–78] and can be ascribed to the increased adsorption of polymer chains on the MWCNT surface which significantly reduces the chain mobility of the PPR. The latter effect is less pronounced at higher temperature (see Table 2) due to weaker interaction between the PPR and the nanofillers.

The gauge factor, defined as the rate at which $\Delta R/R_0$ changes with increasing strain $\varepsilon$, is typically used to evaluate the sensitivity of a piezoresistive material. The gauge factors of the PPR-4, PPR-6 and PPR-8 at 30 °C, 60 °C and 100 °C, were determined by evaluating the slopes of the $\Delta R/R_0$ vs. $\varepsilon$ plots over the range of $0 \leq \varepsilon \leq 0.2$ in Fig. 5b, d and 5f, respectively, and the obtained values are plotted in Fig. 6 and listed in Table 2. At a temperature of 30 °C, the gauge factor decreases with increasing MWCNT loading (see Fig. 6a), reporting a gauge factor of 27.8 for the PPR-4. In contrast, opposite trends are observed at 60 °C (see Fig. 6b) where PPR-8 possesses a remarkably high gauge factor of 395, indicating a significant increase in the sensitivity of the MWCNT/PPR composite with increasing temperature between 30 and 60 °C. With

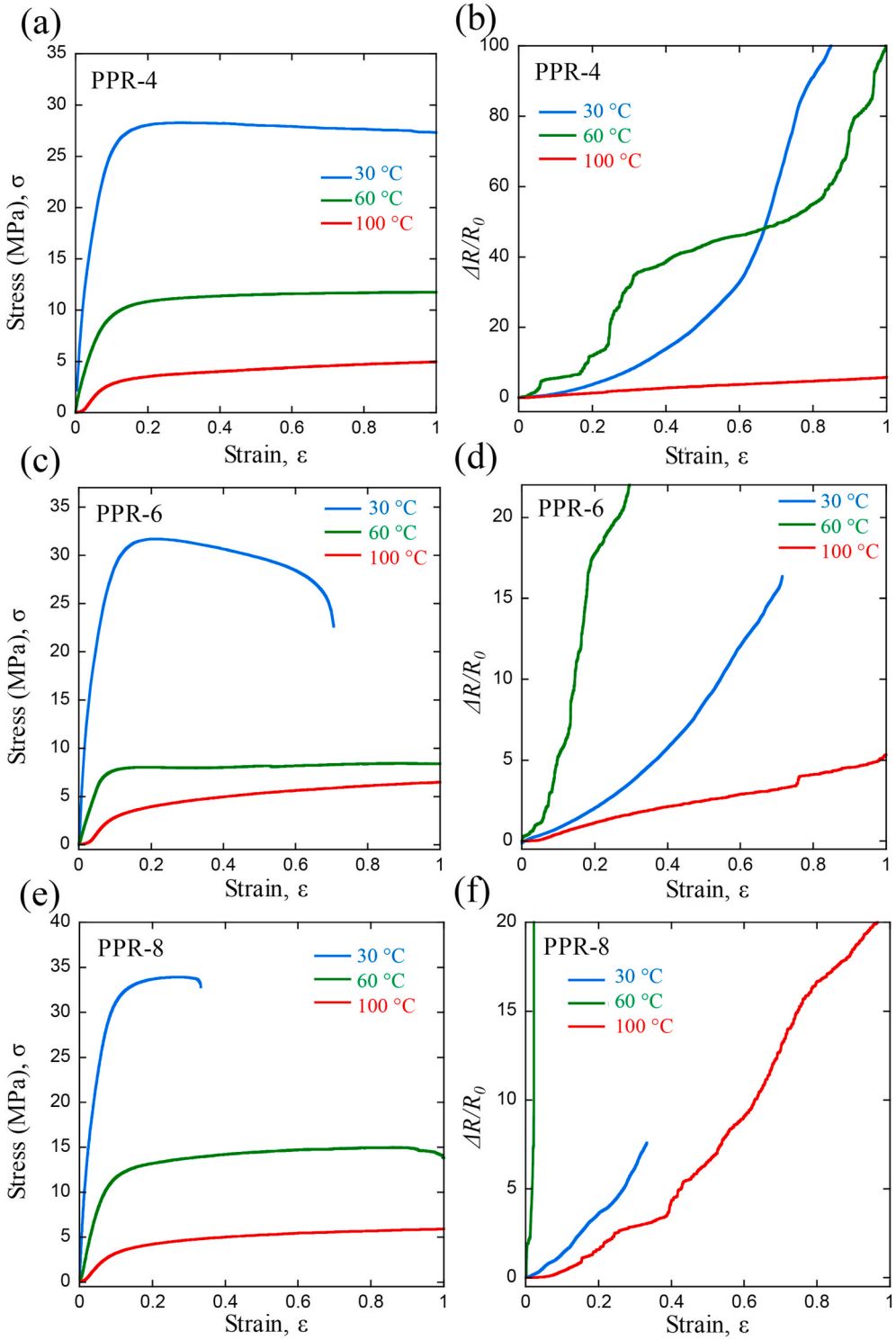


**Fig. 5.** Mechanical and piezoresistive responses of MWCNT/PPR composites under isothermal conditions at 30 °C, 60 °C and 100 °C: (a)–(b) PPR-4; (c)–(d) PPR-6; (e)–(f) PPR-8.

further increase temperature, the sensitivity decreases due to the limited thermal stability of the polymer matrix which fails to support the percolating network of nanofillers. Note that, for a given MWCNT content in PPR matrix, the gauge factor increases with increasing temperature up until 60 °C. This is because the electron tunneling and hopping, both thermally-assisted and activated by mechanical deformation of the PPR matrix, significantly increase the piezoresistance with increase in temperature in this range. It is clear from Fig. 6 that the gauge factors of the MWCNT/PPR composites are very sensitive to variations of temperature within the range of 30–100 °C. Strong thermo-resistive and thermo-piezoresistive characteristics of MWCNT/PPR composites enable the development of smart nanocomposites, for thermal and thermo-piezoresistive sensing applications.

**Table 2**
Mechanical and piezoresistive properties of MWCNT/PPR composites at various temperatures.

| Sample designation | Temperature (°C) | Young's modulus (MPa) | Ultimate strength (MPa) | Failure strain (%) | Gauge factor |
|---|---|---|---|---|---|
| PPR-4 | 30 | 518 | 28.3 | 120 | 27.8 |
| | 60 | 150 | >12.9 | >400 | 52.3 |
| | 100 | 30 | >6.4 | >400 | 6.9 |
| PPR-6 | 30 | 635 | 31.7 | 65 | 20.7 |
| | 60 | 119 | 8.45 | 140 | 93.4 |
| | 100 | 27 | >9.1 | >400 | 6.6 |
| PPR-8 | 30 | 741 | 33.76 | 33 | 17.1 |
| | 60 | 172 | 15.0 | 180 | 395.0 |
| | 100 | 35 | >7.5 | >400 | 9.0 |

### 3.4. Material property chart for thermo-resistive sensing

We proceed to compare the TCR values of our MWCNT/PPR composites to those reported in the current literature. Fig. 7a presents a material property map in the TCR – temperature space where the blue and green fields represent the range of data reported in previous studies for polymer-based nanocomposites and CNT-based thermistors, respectively, while the pink field shows the property range of the MWCNT/PPR reported in this study. It is important to note that Fig. 7 includes data from only those studies where numerical values of TCR were explicitly given (see Table S1, Supplementary Information). Currently, the data is very limited in the high temperature range (i.e. beyond 150 °C), due to the limited thermal stability of the polymer matrix which fails to support the percolating network of nanofillers at elevated temperatures. The figure also shows that the TCR values of polymer-nanocomposites can be positive or negative, due to the competition between thermal fluctuation-induced tunneling (causing negative TCR) and the widening of tunneling gaps between adjacent CNTs driven by thermal expansion of the polymer matrix (causing positive TCR) [53,54,61]. In comparison with data available in the literature, the 3D printed MWCNT/PPR composites reported here exhibit superior thermo-resistive sensitivity, which can be attributed to the alignment of MWCNTs during extrusion of the composite through the nozzle of the 3D printer.

Fig. 7b compares the gauge factors of the MWCNT/PPR reported in

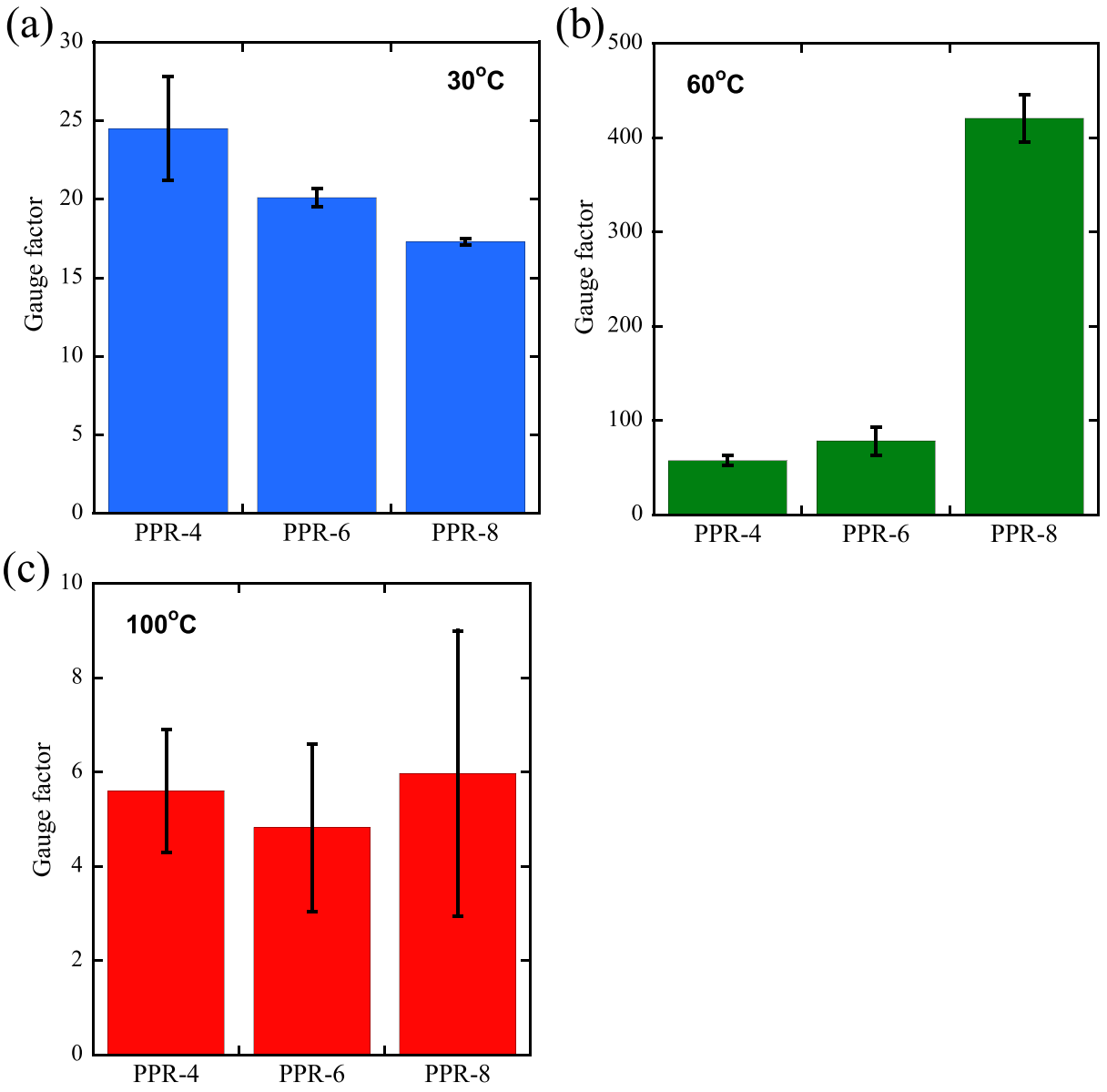


**Fig. 6.** Piezoresistive strain sensing: Gauge factors of MWCNT/PPR composites at three different temperatures: (a) 30 °C, (b) 60 °C and (c) 100 °C.

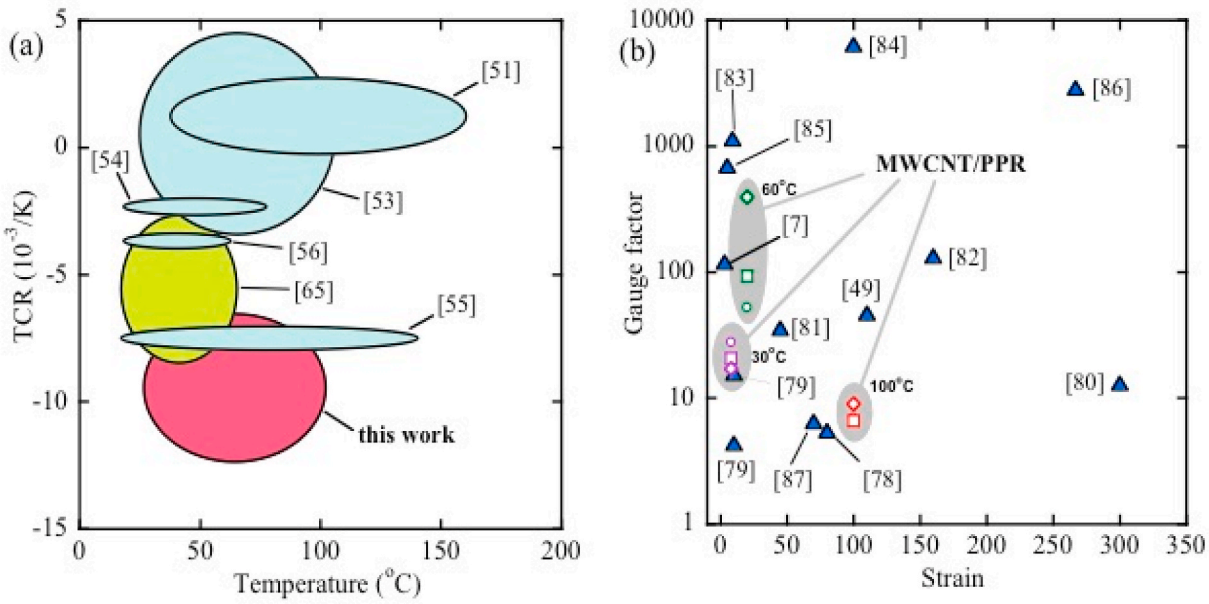


**Fig. 7.** (a) TCR vs. temperature chart showing the property space of nanocomposites (blue fields), CNT-based thermistors (green fields) and the MWCNT/PPR composites reported here (pink fields); (b) Gauge factors of PPR-4 (circles), PPR-6 (squares) and PPR-8 (diamonds) at various temperatures compared to those reported in the literature (triangles).

this study at various temperatures with those of extant works on polymer composites filled with carbon nanostructures at room temperature. The circles (PPR-4), squares (PPR-6) and diamonds (PPR-8) indicate the gauge factors of our study at different temperatures. Fig. 7b further shows that our composite has higher thermo-piezoresistive sensitivity (gauge factor of 395 at 60 °C), demonstrating the potential of our AM-enabled MWCNT/PPR composites for self-sensing both temperature and strain and/or damage state. It is important to note that Fig. 7b includes data from only those studies where numerical values of gauge factor were explicitly given (see Table S2, Supplementary Information). Fig. 7b (Table S1, Supplementary Information) also shows that the gauge factors of polymer-nanocomposites are varying from 0.91 to 120 and the gauge factor exclusively depends on filler type, polymer matrix and morphology of measured samples (foam, fibre, etc.) [7,50,79–88].

## 4. Conclusions

In this study, we experimentally explored the coupling between the electrical resistance and temperature, and the coupling between piezoresistance and temperature of MWCNT/PPR composites enabled via FFF additive manufacturing. The filament feedstocks were fabricated by melt blending neat PPR with a predetermined amount of MWCNTs (either 4, 6 or 8 wt%) in a twin-screw extruder. The thermo-resistive response of the MWCNT/PPR composites was measured under constrained and unconstrained heating from approximately 30-100 °C. For all MWCNT concentrations considered here, negative temperature coefficients of resistivity were reported for both constrained and unconstrained heating, as a consequence of thermal fluctuation-induced tunneling at MWCNT junctions. Although the MWCNT/PPR composites exhibit a very low coefficient of thermal expansion ($\alpha < 0.4 \times 10^{-6}$/°C), measurable thermal stresses were induced in the specimens under constrained heating which were found to relax as the temperature increased. The TCR values measured under constrained conditions were found to be significantly lower than those obtained with unconstrained specimens, suggesting that the segmental chain motion, associated with the stress relaxation of the mechanically constrained PPR matrix above the glass transition temperature, can have a significant effect on the tunneling resistance of the MWCNT network. The highest thermo-resistive sensitivity was observed for the composite with the lowest MWCNT concentration (4 wt%), reporting TCR = $-12{,}800 \times 10^{-6}$/°C, which is higher in magnitude than that of other polymer nanocomposites reported in the literature.

It was also found that the inclusion of MWCNTs in the polymer resulted in a significant stiffening and strengthening effect with a concomitant reduction in ductility (or failure strain). Furthermore, the MWCNT/PPR composites evince pronounced piezoresistive behavior under tensile loading which was found to be highly sensitive to temperature. The gauge factors of MWCNT/PPR composites increased substantially (up to one order of magnitude) after heating the material from 30 °C to 60 °C, and reduced again below their room temperature values when the temperature reached 100 °C, which is likely to be caused by changes in the segmental mobility that affects the morphology and tunneling resistance of the MWCNT network during mechanical straining. Our study further shows higher thermo-piezoresistive sensitivity (gauge factor of 395 at 60 °C), demonstrating the potential of our AM-enabled MWCNT/PPR composites for self-sensing both temperature and strain/damage state. The multi-functionalities of 3D printed MWCNT/PPR composites demonstrated in this study can be seen as critical enablers for the development of innovative sensing technologies. However, hysteresis effects during thermal cycling, as well as the response time to step changes in temperature, are important aspects for most practical applications. These aspects are left to a subsequent study.

## CRediT authorship contribution statement

**Pawan Verma:** Investigation, Writing - original draft. **Andreas Schiffer:** Formal analysis, Writing - original draft. **S. Kumar:** Conceptualization, Methodology, Formal analysis, Writing - original draft.

## Declaration of competing interest

The authors declare that they have no known competing financial interests or personal relationships that could have appeared to influence the work reported in this paper.

## Acknowledgements

Authors would like to thank Abu Dhabi National Oil Company for

providing the research grant (Award No: EX2016-000010). This work was partially funded by Khalifa University of Science and Technology through the Competitive Internal Research Award (CIRA) [grant number CIRA-2018-128]. SK would like to thank the University of Glasgow for the start-up grant.

## Appendix A. Supplementary data

Supplementary data to this article can be found online at https://doi.org/10.1016/j.polymertesting.2020.106961.

## References

[1] S. Yuan, J. Bai, C.K. Chua, J. Wei, K. Zhou, Highly enhanced thermal conductivity of thermoplastic nanocomposites with a low mass fraction of MWCNTs by a facilitated latex approach, Compos. Appl. Sci. Manuf. 90 (2016) 699–710.
[2] R. Megha, F.A. Ali, Y. Ravikiran, C. Ramana, A.K. Kumar, D. Mishra, et al., Conducting polymer nanocomposite based temperature sensors: a review, Inorg. Chem. Commun. 98 (2018) 11–28.
[3] C. Li, E.T. Thostenson, T.-W. Chou, Sensors and actuators based on carbon nanotubes and their composites: a review, Compos. Sci. Technol. 68 (6) (2008) 1227–1249.
[4] A. de la Vega, J. Sumfleth, H. Wittich, K. Schulte, Time and temperature dependent piezoresistance of carbon nanofiller/polymer composites under dynamic load, J. Mater. Sci. 47 (6) (2012) 2648–2657.
[5] S. Gong, Y. Wang, Z. Xiao, Z. Li, Z.X. Wang, R.S. Lei, et al., Effect of temperature on the electrical property of epoxy composites with carbon nanotube, Compos. Sci. Technol. 149 (2017) 48–54.
[6] S. Kumar, T.K. Gupta, K.M. Varadarajan, Strong, stretchable and ultrasensitive MWCNT/TPU nanocomposites for piezoresistive strain sensing, Compos. B Eng. 177 (2019) 107285.
[7] S.P. Patole, S.K. Reddy, A. Schiffer, K. Askar, B.G. Prusty, S. Kumar, Piezoresistive and mechanical characteristics of graphene foam nanocomposites, ACS Applied Nano Materials 2 (3) (2019) 1402–1411.
[8] T.K. Gupta, M. Choosri, K.M. Varadarajan, S. Kumar, Self-sensing and mechanical performance of CNT/GNP/UHMWPE biocompatible nanocomposites, J. Mater. Sci. 53 (11) (2018) 7939–7952.
[9] S.K. Reddy, S. Kumar, K.M. Varadarajan, P.R. Marpu, T.K. Gupta, M. Choosri, Strain and damage-sensing performance of biocompatible smart CNT/UHMWPE nanocomposites, Mater. Sci. Eng. C 92 (2018) 957–968.
[10] J.N. Coleman, U. Khan, W.J. Blau, Y.K. Gun'ko, Small but strong: a review of the mechanical properties of carbon nanotube–polymer composites, Carbon 44 (9) (2006) 1624–1652.
[11] P. Verma, P. Saini, V. Choudhary, Designing of carbon nanotube/polymer composites using melt recirculation approach: effect of aspect ratio on mechanical, electrical and EMI shielding response, Mater. Des. (2015).
[12] S. Berretta, R. Davies, Y.T. Shyng, Y. Wang, O. Ghita, Fused Deposition Modelling of high temperature polymers: exploring CNT PEEK composites, Polym. Test. 63 (2017) 251–262.
[13] N. Hu, H. Fukunaga, S. Atobe, Y. Liu, J. Li, Piezoresistive strain sensors made from carbon nanotubes based polymer nanocomposites, Sensors 11 (11) (2011) 10691–10723.
[14] H.W. Tan, J. An, C.K. Chua, T. Tran, Metallic nanoparticle inks for 3D printing of electronics, Advanced Electronic Materials 5 (5) (2019) 1800831.
[15] H.W. Tan, N. Saengchairat, G.L. Goh, J. An, C.K. Chua, T. Tran, Induction sintering of silver nanoparticle inks on polyimide substrates, Advanced Materials Technologies 5 (1) (2020) 1900897.
[16] J. Gardan, Smart materials in additive manufacturing: state of the art and trends, Virtual Phys. Prototyp. 14 (1) (2019) 1–18.
[17] A.Y. Lee, J. An, C.K. Chua, Two-way 4D printing: a review on the reversibility of 3D-printed shape memory materials, Engineering 3 (5) (2017) 663–674.
[18] W.L. Ng, C.K. Chua, Y.-F. Shen, Print me an organ! Why we are not there yet, Prog. Polym. Sci. 97 (2019) 101145.
[19] S. Kumar, B.L. Wardle, M.F. Arif, J. Ubaid, Stress reduction of 3D printed compliance-tailored multilayers, Adv. Eng. Mater. 20 (1) (2018) 1700883.
[20] Y.Y.C. Choong, S. Maleksaeedi, H. Eng, S. Yu, J. Wei, P.-C. Su, High speed 4D printing of shape memory polymers with nanosilica, Applied Materials Today 18 (2020) 100515.
[21] S. Yuan, F. Shen, C.K. Chua, K. Zhou, Polymeric composites for powder-based additive manufacturing: materials and applications, Prog. Polym. Sci. 91 (2019) 141–168.
[22] C.W. Hull, Apparatus for Production of Three-Dimensional Objects by Stereolithography, Google Patents, 1986.
[23] S. Kumar, B.L. Wardle, M.F. Arif, Strength and performance enhancement of bonded joints by spatial tailoring of adhesive compliance via 3D printing, ACS Appl. Mater. Interfaces 9 (1) (2017) 884–891.
[24] S. Kumar, J. Ubaid, R. Abishera, A. Schiffer, V.S. Deshpande, Tunable energy absorption characteristics of architected honeycombs enabled via additive manufacturing, ACS Appl. Mater. Interfaces 11 (45) (2019) 42549–42560.
[25] J. Porter, T. Cain, S. Fox, P. Harvey, Influence of infill properties on flexural rigidity of 3D-printed structural members, Virtual Phys. Prototyp. 14 (2) (2019) 148–159.
[26] Y. Weng, M. Li, Z. Liu, W. Lao, B. Lu, D. Zhang, et al., Printability and fire performance of a developed 3D printable fibre reinforced cementitious composites under elevated temperatures, Virtual Phys. Prototyp. 14 (3) (2019) 284–292.
[27] P. Bedi, R. Singh, I. Ahuja, Effect of SiC/Al2O3 particle size reinforcement in recycled LDPE matrix on mechanical properties of FDM feed stock filament, Virtual Phys. Prototyp. 13 (4) (2018) 246–254.
[28] K. Gnanasekaran, T. Heijmans, S. Van Bennekom, H. Woldhuis, S. Wijnia, G. de With, et al., 3D printing of CNT-and graphene-based conductive polymer nanocomposites by fused deposition modeling, Applied materials today 9 (2017) 21–28.
[29] M.F. Arif, H. Alhashmi, K.M. Varadarajan, J.H. Koo, A.J. Hart, S. Kumar, Multifunctional performance of carbon nanotubes and graphene nanoplatelets reinforced PEEK composites enabled via FFF additive manufacturing, Compos. B Eng. 184 (2020) 107625.
[30] A. Mora, P. Verma, S. Kumar, Electrical conductivity of CNT/polymer composites: 3D printing, measurements and modeling, Compos. B Eng. 183 (2020) 107600.
[31] A.R. Rajkumar, K. Shanmugam, Additive manufacturing-enabled shape transformations via FFF 4D printing, J. Mater. Res. 33 (24) (2018) 4362–4376.
[32] M.F. Arif, S. Kumar, K.M. Varadarajan, W.J. Cantwell, Performance of biocompatible PEEK processed by fused deposition additive manufacturing, Mater. Des. 146 (2018) 249–259.
[33] J. Schneider, S. Kumar, Multiscale characterization and constitutive parameters identification of polyamide (PA12) processed via selective laser sintering, Polym. Test. 86 (2020) 106357.
[34] S. Yuan, Y. Zheng, C.K. Chua, Q. Yan, K. Zhou, Electrical and thermal conductivities of MWCNT/polymer composites fabricated by selective laser sintering, Compos. Appl. Sci. Manuf. 105 (2018) 203–213.
[35] W. Yu, S.L. Sing, C.K. Chua, X. Tian, Influence of re-melting on surface roughness and porosity of AlSi10Mg parts fabricated by selective laser melting, J. Alloys Compd. 792 (2019) 574–581.
[36] W.H. Yu, S.L. Sing, C.K. Chua, C.-N. Kuo, X.L. Tian, Particle-reinforced metal matrix nanocomposites fabricated by selective laser melting: a state of the art review, Prog. Mater. Sci. 104 (2019) 330–379.
[37] Y. Li, K. Zhou, P. Tan, S.B. Tor, C.K. Chua, K.F. Leong, Modeling temperature and residual stress fields in selective laser melting, Int. J. Mech. Sci. 136 (2018) 24–35.
[38] C. Kuo, C. Chua, P. Peng, Y. Chen, S. Sing, S. Huang, et al., Microstructure evolution and mechanical property response via 3D printing parameter development of Al–Sc alloy, Virtual Phys. Prototyp. 15 (1) (2020) 120–129.
[39] R.D. Farahani, M. Dubé, D. Therriault, Three-dimensional printing of multifunctional nanocomposites: manufacturing techniques and applications, Adv. Mater. 28 (28) (2016) 5794–5821.
[40] K. Gnanasekaran, T. Heijmans, S. van Bennekom, H. Woldhuis, S. Wijnia, G. de With, et al., 3D printing of CNT- and graphene-based conductive polymer nanocomposites by fused deposition modeling, Applied Materials Today 9 (2017) 21–28.
[41] X. Wang, M. Jiang, Z. Zhou, J. Gou, D. Hui, 3D printing of polymer matrix composites: a review and prospective, Compos. B Eng. 110 (2017) 442–458.
[42] O.A. Mohamed, S.H. Masood, J.L. Bhowmik, Parametric Analysis of the Build Cost for FDM Additive Processed Parts Using Response Surface Methodology. Reference Module in Materials Science and Materials Engineering, Elsevier, 2016.
[43] G.M. Rizvi, C.T. Bellehumeur, P. Gu, Q. Sun, Effect of processing conditions on the bonding quality of FDM polymer filaments, Rapid Prototyp. J. 14 (2) (2008) 72–80.
[44] B. Tymrak, M. Kreiger, J.M. Pearce, Mechanical properties of components fabricated with open-source 3-D printers under realistic environmental conditions, Mater. Des. 58 (2014) 242–246.
[45] P. Tran, T.D. Ngo, A. Ghazlan, D. Hui, Bimaterial 3D printing and numerical analysis of bio-inspired composite structures under in-plane and transverse loadings, Compos. B Eng. 108 (2017) 210–223.
[46] R. Melnikova, A. Ehrmann, K. Finsterbusch, 3D printing of textile-based structures by Fused Deposition Modelling (FDM) with different polymer materials, in: IOP Conference Series: Materials Science and Engineering, IOP publishing, 2014, 012018.
[47] B. Caulfield, P. McHugh, S. Lohfeld, Dependence of mechanical properties of polyamide components on build parameters in the SLS process, J. Mater. Process. Technol. 182 (1–3) (2007) 477–488.
[48] C.R. Garcia, J. Correa, D. Espalin, J.H. Barton, R.C. Rumpf, R. Wicker, et al., 3D printing of anisotropic metamaterials, Progress In Electromagnetics Research 34 (2012) 75–82.
[49] M.R. Dusseiller, D. Schlaepfer, M. Koch, R. Kroschewski, M. Textor, An inverted microcontact printing method on topographically structured polystyrene chips for arrayed micro-3-D culturing of single cells, Biomaterials 26 (29) (2005) 5917–5925.
[50] M.F. Arif, S. Kumar, T.K. Gupta, K.M. Varadarajan, Strong linear-piezoresistive-response of carbon nanostructures reinforced hyperelastic polymer nanocomposites, Compos. Appl. Sci. Manuf. 113 (2018) 141–149.
[51] F. Avilés, A.I. Oliva-Avilés, M. Cen-Puc, Piezoresistivity, strain, and damage self-sensing of polymer composites filled with carbon nanostructures, Adv. Eng. Mater. (2018) 1701159.
[52] K.L. Lasater, E.T. Thostenson, In situ thermoresistive characterization of multifunctional composites of carbon nanotubes, Polymer 53 (23) (2012) 5367–5374.
[53] M. Cen-Puc, A. Oliva-Avilés, F. Avilés, Thermoresistive mechanisms of carbon nanotube/polymer composites, Phys. E Low-dimens. Syst. Nanostruct. 95 (2018) 41–50.
[54] M. Cen-Puc, G. Pool, A. Oliva-Avilés, A. May-Pat, F. Avilés, Experimental investigation of the thermoresistive response of multiwall carbon nanotube/

polysulfone composites under heating-cooling cycles, Compos. Sci. Technol. 151 (2017) 34–43.
[55] K.S. Karimov, M.T.S. Chani, F.A. Khalid, Carbon nanotubes film based temperature sensors, Phys. E Low-dimens. Syst. Nanostruct. 43 (9) (2011) 1701–1703.
[56] M. Mohiuddin, S. Hoa, Temperature dependent electrical conductivity of CNT–PEEK composites, Compos. Sci. Technol. 72 (1) (2011) 21–27.
[57] G. Matzeu, A. Pucci, S. Savi, M. Romanelli, F. Di Francesco, A temperature sensor based on a MWCNT/SEBS nanocomposite, Sens. Actuators, A 178 (2012) 94–99.
[58] Y. Zeng, G. Lu, H. Wang, J. Du, Z. Ying, C. Liu, Positive temperature coefficient thermistors based on carbon nanotube/polymer composites, Sci. Rep. 4 (2014) 6684.
[59] H. Nakano, K. Shimizu, S. Takahashi, A. Kono, T. Ougizawa, H. Horibe, Resistivity–temperature characteristics of filler-dispersed polymer composites, Polymer 53 (26) (2012) 6112–6117.
[60] M. Lisunova, Y.P. Mamunya, N. Lebovka, A. Melezhyk, Percolation behaviour of ultrahigh molecular weight polyethylene/multi-walled carbon nanotubes composites, Eur. Polym. J. 43 (3) (2007) 949–958.
[61] J. Shen, S. Buschhorn, J.T.M. De Hosson, K. Schulte, B. Fiedler, Pressure and temperature induced electrical resistance change in nano-carbon/epoxy composites, Compos. Sci. Technol. 115 (2015) 1–8.
[62] T. Dinh, H.-P. Phan, A. Qamar, P. Woodfield, N.-T. Nguyen, D.V. Dao, Thermoresistive effect for advanced thermal sensors: fundamentals, design considerations, and applications, Journal of Microelectromechanical Systems 26 (5) (2017) 966–986.
[63] Z.D. Xiang, T. Chen, Z.M. Li, X.C. Bian, Negative temperature coefficient of resistivity in lightweight conductive carbon nanotube/polymer composites, Macromol. Mater. Eng. 294 (2) (2009) 91–95.
[64] R. Megha, F.A. Ali, Y.T. Ravikiran, C.H.V.V. Ramana, A.B.V. Kiran Kumar, D. K. Mishra, et al., Conducting polymer nanocomposite based temperature sensors: a review, Inorg. Chem. Commun. 98 (2018) 11–28.
[65] A.E. Aliev, C. Guthy, M. Zhang, S. Fang, A.A. Zakhidov, J.E. Fischer, et al., Thermal transport in MWCNT sheets and yarns, Carbon 45 (15) (2007) 2880–2888.
[66] S. Selvarasah, A. Busnaina, M. Dokmeci, Design, fabrication, and characterization of three-dimensional single-walled carbon nanotube assembly and applications as thermal sensors, IEEE Trans. Nanotechnol. 10 (1) (2010) 13–20.
[67] P. Verma, P. Saini, R.S. Malik, V. Choudhary, Excellent electromagnetic interference shielding and mechanical properties of high loading carbon-nanotubes/polymer composites designed using melt recirculation equipped twin-screw extruder, Carbon 89 (2015) 308–317.
[68] P. Hall, The effect of expansion mismatch on temperature coefficient of resistance of thin films, Appl. Phys. Lett. 12 (6) (1968) 212.
[69] B. Verma, S. Sharma, Effect of thermal strains on the temperature coefficient of resistance, Thin Solid Films 5 (4) (1970) R44–R46.
[70] M. Cen-Puc, A.I. Oliva-Avilés, F. Avilés, Thermoresistive mechanisms of carbon nanotube/polymer composites, Phys. E Low-dimens. Syst. Nanostruct. 95 (2018) 41–50.
[71] V.S. Turkani, D. Maddipatla, B.B. Narakathu, B.J. Bazuin, M.Z. Atashbar, A carbon nanotube based NTC thermistor using additive print manufacturing processes, Sens. Actuators, A 279 (2018) 1–9.
[72] H.C. Neitzert, A. Sorrentino, L. Vertuccio, Epoxy/MWCNT composite based temperature sensor with linear characteristics, in: P. Malcovati, A. Baschirotto, A. d'Amico, C. Natale (Eds.), Sensors and Microsystems, Springer Netherlands, Dordrecht, 2010, pp. 241–245.
[73] P. Verma, M. Verma, A. Gupta, S.S. Chauhan, R.S. Malik, V. Choudhary, Multi walled carbon nanotubes induced viscoelastic response of polypropylene copolymer nanocomposites: effect of filler loading on rheological percolation, Polym. Test. 55 (2016) 1–9.
[74] P.-G. Ren, J. Wang, Q. Fan, S. Yang, Z.-Q. Wu, D.-X. Yan, et al., Synergetic toughening effect of carbon nanotubes and β-nucleating agents on the polypropylene random copolymer/styrene-ethylene-butylene-styrene block copolymer blends, Polymers 11 (1) (2019) 29.
[75] Z.-J. Wang, D.-J. Kwon, G.-Y. Gu, H.-S. Kim, D.-S. Kim, C.-S. Lee, et al., Mechanical and interfacial evaluation of CNT/polypropylene composites and monitoring of damage using electrical resistance measurements, Compos. Sci. Technol. 81 (2013) 69–75, 0.
[76] X.-L. Xie, Y.-W. Mai, X.-P. Zhou, Dispersion and alignment of carbon nanotubes in polymer matrix: a review, Mater. Sci. Eng. R Rep. 49 (4) (2005) 89–112.
[77] M.-K. Yeh, N.-H. Tai, J.-H. Liu, Mechanical behavior of phenolic-based composites reinforced with multi-walled carbon nanotubes, Carbon 44 (1) (2006) 1–9.
[78] A. Pantano, G. Modica, F. Cappello, Multiwalled carbon nanotube reinforced polymer composites, Mater. Sci. Eng., A 486 (1–2) (2008) 222–227.
[79] J.-H. Kong, N.-S. Jang, S.-H. Kim, J.-M. Kim, Simple and rapid micropatterning of conductive carbon composites and its application to elastic strain sensors, Carbon 77 (2014) 199–207.
[80] Y. Zheng, Y. Li, Z. Li, Y. Wang, K. Dai, G. Zheng, et al., The effect of filler dimensionality on the electromechanical performance of polydimethylsiloxane based conductive nanocomposites for flexible strain sensors, Compos. Sci. Technol. 139 (2017) 64–73.
[81] Y. Zheng, Y. Li, K. Dai, Y. Wang, G. Zheng, C. Liu, et al., A highly stretchable and stable strain sensor based on hybrid carbon nanofillers/polydimethylsiloxane conductive composites for large human motions monitoring, Compos. Sci. Technol. 156 (2018) 276–286.
[82] X. Wang, J. Li, H. Song, H. Huang, J. Gou, Highly stretchable and wearable strain sensor based on printable carbon nanotube layers/polydimethylsiloxane composites with adjustable sensitivity, ACS Appl. Mater. Interfaces 10 (8) (2018) 7371–7380.
[83] D. Cho, J. Park, J. Kim, T. Kim, J. Kim, I. Park, et al., Three-dimensional continuous conductive nanostructure for highly sensitive and stretchable strain sensor, ACS Appl. Mater. Interfaces 9 (20) (2017) 17369–17378.
[84] B. Nie, X. Li, J. Shao, X. Li, H. Tian, D. Wang, et al., Flexible and transparent strain sensors with embedded multiwalled carbon nanotubes meshes, ACS Appl. Mater. Interfaces 9 (46) (2017) 40681–40689.
[85] S. Kumar, T.K. Gupta, K. Varadarajan, Strong, stretchable and ultrasensitive MWCNT/TPU nanocomposites for piezoresistive strain sensing, Compos. B Eng. 177 (2019) 107285.
[86] H. Montazerian, A. Dalili, A. Milani, M. Hoorfar, Piezoresistive sensing in chopped carbon fiber embedded PDMS yarns, Compos. B Eng. 164 (2019) 648–658.
[87] S. Yu, X. Wang, H. Xiang, L. Zhu, M. Tebyetekerwa, M. Zhu, Superior piezoresistive strain sensing behaviors of carbon nanotubes in one-dimensional polymer fiber structure, Carbon 140 (2018) 1–9.
[88] S. Wu, J. Zhang, R.B. Ladani, A.R. Ravindran, A.P. Mouritz, A.J. Kinloch, et al., Novel electrically conductive porous PDMS/carbon nanofiber composites for deformable strain sensors and conductors, ACS Appl. Mater. Interfaces 9 (16) (2017) 14207–14215.